

Comparison of new RANS-LES hybrid methods on a tandem cylinder problem using rough meshes

L. Hájek^{a,*}, J. Karel^a, M. Klíma^a, D. Trdlička^a

^a*Department of Technical Mathematics, Faculty of Mechanical Engineering, Czech Technical University in Prague, Karlovo náměstí 13, 121 35 Praha 2, Czech Republic*

Received 19 March 2024; accepted 6 December 2024

Abstract

Detached eddy simulation (DES), delayed DES (DDES) and improved DDES (IDDES) hybrid RANS-LES turbulence models based on the Menter's Shear Stress Transport (SST) model as well as the DES variant of the Kok's Turbulent/Non-Turbulent model (TNT), Extra-Large Eddy Simulation (X-LES), and its newly proposed delayed and improved delayed variants (DX-LES and IDX-LES) along with the base RANS methods are compared in this paper. The comparison is made on a flow around tandem cylinders, on which mainly hybrid methods based on the one-equation Spalart-Almaras model were previously tested. The proposed models show DDES and IDDES with a different approach from the SST-based two-equation methods, which potentially improves the results and, in the case of the TNT-based DDES variant, only the blending function is dependent of the distance from the wall.

© 2024 University of West Bohemia.

Keywords: CFD, turbulence modeling, Orion software, RANS-LES hybrid methods, DES, vortex shedding

1. Introduction

Resolving turbulent flow in CFD plays an important role in engineering, but comes with a number of challenges. For example, neither of two of the most common approaches is without flaws: The approaches based solely on the Reynolds-averaged Navier-Stokes (RANS) equations, while usually being one of the less computationally expensive methods, do not resolve a satisfying range of turbulent length scales for all applications, while the large eddy simulation (LES) resolves wider range of turbulent length scales, but at the cost of increased computational demands. This is one of the main reasons why hybrid RANS-LES methods have been used more and more frequently in recent years.

Detached eddy simulation (DES), as first formulated by Spalart et al. in [21], is probably the most basic hybrid RANS-LES method, but its binary switching between the two modes can become problematic. It can lead to effects such as the so-called grid induced separation, which can happen when LES mode is employed in regions close to walls where RANS mode should have been used, as demonstrated by Menter et al. in 2003 [16]. Since then, a delayed variants of DES (DDES) have been developed, introducing a blending function to smooth the transition and prevent problematic switching to LES mode. This approach was also combined with wall-modeled LES (WMLES) to formulate improved DDES (IDDES).

In this paper, the 2003 version of the Menter's Shear Stress Transport (SST) [16] and Kok's Turbulent/Non-Turbulent (TNT) [9] two-equation models are used as the base RANS methods. For the SST model, its DES formulation by Spalart [22] is chosen, while the DDES and IDDES

*Corresponding author. Tel.: +420 224 357 430, e-mail: lukas.hajek@fs.cvut.cz.
<https://doi.org/10.24132/acm.2024.893>

variants are the ones formulated by Gritskevich et al. in [3]. As for the TNT model, only the DES variant was published—the Extra-Large Eddy Simulation method by Kok et al. [10]. The article by Fracassi et al. [1] from 2022 described a delayed version of the original X-LES model, but not without replacing its TNT base RANS method by SST. To stay consistent with the original X-LES version as well as to compare different base RANS methods, the delayed and improved delayed variants of the X-LES model (DX-LES and IDX-LES) newly presented here are all TNT-based.

The chosen test for the comparison of the RANS and hybrid RANS-LES methods is a flow around tandem cylinders proposed by NASA to study aircraft landing gears [6, 7], specifically with two cylinder centres spaced $3.7D$ apart, where D is the diameter of the cylinders. This test case is characterized by the Reynolds number of 166 000 (with D being the characteristic length). In these conditions, the first cylinder causes a continuous vortex shedding, creating a vortex street that is passed onto the second cylinder, where the separated boundary layer reattaches and then separates again and forms another vortex street. This test case was used as a benchmark before in [12] (where mainly hybrid methods based on the Spalart-Almaras one-equation model were tested), EU-project ATAAC [18], for spectral difference method [2], noise investigations and aeroacoustic simulations [8, 11, 13, 14, 24] and also in [15] for Reynolds stress modeling.

2. Mathematical model

Since the considered fluid in the described test case is air, we assume that it behaves according to the thermodynamic model of an ideal gas. Using the Reynolds analogy for the Fourier's law of heat conduction, neglecting the effects of gravity and applying the Reynolds and Favre averaging on the Navier-Stokes equations, the fluid flow is described by the following RANS equations:

$$\frac{\partial \varrho}{\partial t} + \operatorname{div}(\varrho \mathbf{u}) = 0, \quad (1)$$

$$\frac{\partial(\varrho \mathbf{u})}{\partial t} + \operatorname{div}[(\varrho \mathbf{u}) \otimes \mathbf{u}] = \operatorname{div} \boldsymbol{\sigma} + \operatorname{div} \boldsymbol{\tau} - \operatorname{grad} p, \quad (2)$$

$$\begin{aligned} \frac{\partial(\varrho E)}{\partial t} + \operatorname{div}(\varrho \mathbf{u} H) &= \operatorname{div}(\boldsymbol{\tau} \mathbf{u}) + \operatorname{div}\left(\frac{c_p \mu_L}{\operatorname{Pr}} \operatorname{grad} T\right) \\ &+ \operatorname{div}\left[\boldsymbol{\sigma} \mathbf{u} + \left(\mu_L + \frac{\mu_T}{\sigma_k}\right) \operatorname{grad} k + \frac{c_p \mu_T}{\operatorname{Pr}_T} \operatorname{grad} T\right], \quad (3) \end{aligned}$$

where ϱ is the fluid density, t denotes the time, \mathbf{u} represents the vector of fluid velocity, p is the pressure, E is the specific total energy, $H = E + p/\varrho$ is the specific enthalpy, T denotes the fluid temperature, c_p is the heat capacity at constant pressure, Pr and Pr_T represent the Prandtl number and its turbulent counterpart, μ_L and μ_T are the dynamic laminar and eddy viscosity, respectively, σ_k represents a coefficient given by a turbulence model, k denotes the turbulence kinetic energy, $\boldsymbol{\sigma}$ is the viscous stress tensor approximated (assuming that \mathbf{S} is the strain tensor and \mathbf{I} is the identity matrix) as

$$\boldsymbol{\sigma} \approx 2\mu_L \left[\mathbf{S} - \frac{1}{3} \operatorname{div}(\mathbf{u}) \mathbf{I} \right], \quad (4)$$

and $\boldsymbol{\tau}$ denotes the Reynolds stress tensor, approximated, similarly to $\boldsymbol{\sigma}$, by the Boussinesq approximation.

The system (1)–(3) is closed by the equation of state

$$p = (\gamma - 1) \left[\rho E - \frac{1}{2} \rho (u_1^2 + u_2^2 + u_3^2) \right] \quad (5)$$

and one of the above described turbulence models, all being two-equation k - ω models, where ω is the specific turbulence dissipation rate. The equations of methods based on the 2003 SST model [16] are as follows:

$$\frac{\partial(\rho k)}{\partial t} + \text{div}(\rho k \mathbf{u}) = \text{div}[(\mu_L + \sigma_k \mu_T) \text{grad } k] + P - \rho k \frac{\sqrt{k}}{L_T}, \quad (6)$$

$$\frac{\partial(\rho \omega)}{\partial t} + \text{div}(\rho \omega \mathbf{u}) = \text{div}[(\mu_L + \sigma_\omega \mu_T) \text{grad } \omega] + \frac{C_\omega \rho}{\mu_T} P - \beta \rho \omega^2 + (1 - F_1) CD, \quad (7)$$

where L_T is the model length scale (which is the term that determines whether the method is RANS, DES, DDES or IDDES), P denotes the limited production and CD denotes the cross-diffusion, both described in [16], and any model constant ϕ for the SST model is computed as $\phi = F_1 \phi^{(1)} + (1 - F_1) \phi^{(2)}$ by using

$$\begin{aligned} \sigma_k^{(1)} &= 0.85, & \sigma_\omega^{(1)} &= 0.5, & \beta^{(1)} &= 0.075, & C_\omega^{(1)} &= 0.553, \\ \sigma_k^{(2)} &= 1, & \sigma_\omega^{(2)} &= 0.856, & \beta^{(2)} &= 0.0828, & C_\omega^{(2)} &= 0.44. \end{aligned} \quad (8)$$

Using the function F_2 from [16], we can define the eddy viscosity for the SST-based models as

$$\mu_T^{(\text{SST})} = \frac{a_1 \rho k}{\max(a_1 \omega, F_2 S)}, \quad a_1 = 0.31. \quad (9)$$

To define the model length scale L_T , the RANS and LES lengths need to be defined first

$$l_{\text{RANS}} = \frac{\sqrt{k}}{\beta^* \omega}, \quad l_{\text{LES}} = C_{\text{DES}} \Delta, \quad \hat{l}_{\text{LES}} = C_{\text{DES}} \hat{\Delta}, \quad (10)$$

with $\beta^* = 0.09$, Δ is the the maximum length of the cell's edges and C_{DES} is a coefficient calculated for the SST-based models as other model constants of this method using, similarly to (8), $C_{\text{DES}}^{(1)} = 0.78$ and $C_{\text{DES}}^{(2)} = 0.61$, as described in [22], and $\hat{\Delta}$ is the modification of Δ for the improved delayed models utilizing the distance from the nearest wall d_w

$$\hat{\Delta} = \min [C_w \max(d_w, \Delta), \Delta], \quad C_w = 0.15. \quad (11)$$

As briefly mentioned in the previous section, DES methods are known to inadvertently switch to LES mode in regions with small computational cells close to the wall, causing the so-called modeled stress depletion [20], which can potentially lead to premature boundary layer separation, called grid-induced separation [16]. To solve these problems, the DDES model introduces the DDES blending function f_d , ensuring a better and smoother transition between the two modes, defined by Gritskevich et al. [3] as

$$f_d = 1 - \tanh \left[(C_{d1} r_d)^{C_{d2}} \right], \quad (12)$$

where $C_{d1} = 20$, $C_{d2} = 3$, and

$$r_d = \frac{\frac{1}{\rho} (\mu_T + \mu_L)}{\kappa^2 d_w^2 \sqrt{0.5 (S^2 + \Omega^2)}}, \quad \kappa = 0.41, \quad (13)$$

with S being the norm of the strain tensor and Ω the norm of the vorticity tensor.

The IDDES approach introduces WMLES techniques into the DDES formulation, allowing for rapid transition from RANS to LES if the WMLES empirical blending function f_b has large enough value. According to the description by Gritskevich et al. [3], the IDDES blending function \tilde{f} and the function f_b are defined as

$$\begin{aligned} \tilde{f}_d &= \max(1 - f_{dT}, f_b), & f_{dT} &= 1 - \tanh\left[(C_{d1}r_{dT})^{C_{d2}}\right], \\ f_b &= \min[2 \exp(-9\alpha^2), 1.0], & \alpha &= 0.25 - \frac{d_w}{\Delta}, \end{aligned} \quad (14)$$

where the coefficients κ , C_{d1} and C_{d2} are identical to the ones from (12) and (13) for the DDES model. The function r_d from (13) is now replaced by functions r_{dT} and r_{dL} , both of which can be described by the following formula, with f_T and f_L being defined similarly:

$$r_{dT/L} = \frac{\frac{1}{2}\mu_{T/L}}{\kappa^2 d_w^2 \sqrt{0.5(S^2 + \Omega^2)}}, \quad f_{T/L} = \tanh\left[(C_{T/L}^2 r_{dT/L})^{\xi_{T/L}}\right], \quad C_T = 1.87, \quad C_L = 5.0, \quad (15)$$

where $\xi_T = 3$ and $\xi_L = 10$. While only r_{dT} is needed to define the blending function \tilde{f}_d from (14)₁, r_{dL} as well as f_T and f_L are required by the elevating function f_e , which can be written as

$$f_e = f_{e2} \max(f_{e1} - 1, 0), \quad f_{e2} = 1.0 - \max(f_T, f_L), \quad (16)$$

where

$$f_{e1} = \begin{cases} 2 \exp(-11.09\alpha^2) & \text{if } \alpha \geq 0, \\ 2 \exp(-9\alpha^2) & \text{if } \alpha < 0. \end{cases} \quad (17)$$

The purpose of the function f_e is to solve the problem of the so-called log-layer mismatch, a deviation of the modeled wall-shear stress of WMLES methods by approximately 15 %, as described by Nikitin et al. in [17]. Gritskevich et al. also described in [3] a simplified version of the IDDES model without the elevating function (essentially setting $f_e = 0$). This version can be justified, as in this formulation both full and simplified variants give results similarly close to the experimental data, as also confirmed by [3]. However, the results presented here are utilizing the full version, with the elevating function described in (16).

Finally, using the described RANS and LES scales as well as the blending functions, the model length scales L_T of SST, SST-DES, SST-DDES and SST-IDDES methods are defined in Table 1, completing the description of these methods.

Table 1. Model length scales L_T for different methods

Switching	Model length scale	Base model	
RANS only	$L_T = l_{\text{RANS}}$	SST (6)–(7)	TNT (18)–(19)
Binary RANS-LES	$L_T = \min(l_{\text{RANS}}, l_{\text{LES}})$	DES	X-LES
Delayed	$L_T = l_{\text{RANS}} - f_d \max(0, l_{\text{RANS}} - l_{\text{LES}})$	DDES	DX-LES
Improved delayed	$L_T = \tilde{f}_d(1 + f_e)l_{\text{RANS}} + (1 - \tilde{f}_d)l_{\text{LES}}$	IDDES	IDX-LES

For the methods based on the Kok’s TNT method [9], the model equations can be written as

$$\frac{\partial(\varrho k)}{\partial t} + \operatorname{div}(\varrho k \mathbf{u}) = \operatorname{div}[(\mu_L + \sigma_k \mu_T) \operatorname{grad} k] + P_k - \varrho k \frac{\sqrt{k}}{L_T}, \quad (18)$$

$$\frac{\partial(\varrho \omega)}{\partial t} + \operatorname{div}(\varrho \omega \mathbf{u}) = \operatorname{div}[(\mu_L + \sigma_\omega \mu_T) \operatorname{grad} \omega] + P_\omega - \beta \varrho \omega^2 + C_D, \quad (19)$$

where L_T is defined the same way, although with a different value of $C_{\text{DES}} = 5/9$ for the TNT-based models, as in the case of the SST-based methods (RANS length scale corresponds to the TNT RANS model, DES scale to the X-LES method, DDES scale to DX-LES and the IDDES length scale to the IDX-LES model), as described in Table 1, P_k is the production of k , which is in this case limited by the Wallin’s modification [23] to prevent unnaturally large growth of turbulent values

$$P_k = \min \left(\tilde{P}_k, \varrho k \sqrt{\frac{\tilde{P}_k}{\mu_T}} \right), \quad \tilde{P}_k = \sum_{i,j} \tau_{ij} \frac{\partial u_j}{\partial x_i}, \quad (20)$$

the production term P_ω is given by

$$P_\omega = \frac{\alpha_\omega \omega}{k} P_k \quad (21)$$

and C_D denotes the cross-diffusion term described in [9]. It is also worth noting that the TNT-based XLES method is, unlike the SST-based models and many others including the original DES model [21] based on the one-equation Spalart-Almaras model [19], independent of the distance from the nearest wall, so for the DX-LES only the blending function depends on this parameter. Finally, the eddy viscosity for the TNT-based methods is defined using L_T as

$$\mu_T^{(\text{TNT})} = \beta^* \varrho \sqrt{k} L_T. \quad (22)$$

3. Numerical methods

The computations are done by in-house parallel CFD software Orion. It uses implicit formulation of the finite volume method to solve the RANS equations (1)–(3) separately from the two equations of the given turbulence model. If left and right sides of the equations are respected, both systems can be written as

$$\frac{\partial \mathbf{W}}{\partial t} + \operatorname{div} \mathbf{F}_C(\mathbf{W}) = \operatorname{div} \mathbf{F}_D(\mathbf{W}) + \mathbf{Q}(\mathbf{W}), \quad (23)$$

where \mathbf{W} is the vector of conservative variables (of five or two components, depending on the system), \mathbf{F}_C are the convective fluxes, \mathbf{F}_D denotes the diffusive fluxes and \mathbf{Q} is the source term.

For the spatial discretization, the HLLC scheme is utilized for (1)–(3). The results of this scheme can be further improved for lower fluid velocities by using the modification of the HLLC scheme by Holman [4] and less dissipative scheme for LES regions. Least square reconstruction with the Barth-Jespersen limiter is used for calculation of all convective fluxes. The derivatives required by the implicit scheme are resolved analytically, but only in the two neighbor cells of the cell face where the flux is computed, while Jacobians in wider surroundings are discarded. As for the diffusive fluxes, gradients are resolved by using values at points of ”diamond cell” around the given cell face, while the least square method for the values in mesh nodes is utilized.

The time discretization is done by using the second-order backward differentiation formula (BDF2). Dual time-stepping is also used by utilizing the first-order BDF. Additionally, local time stepping is used for the iterative process in dual time. The resulting linear system in each time step is then resolved by the generalized minimal residual method.

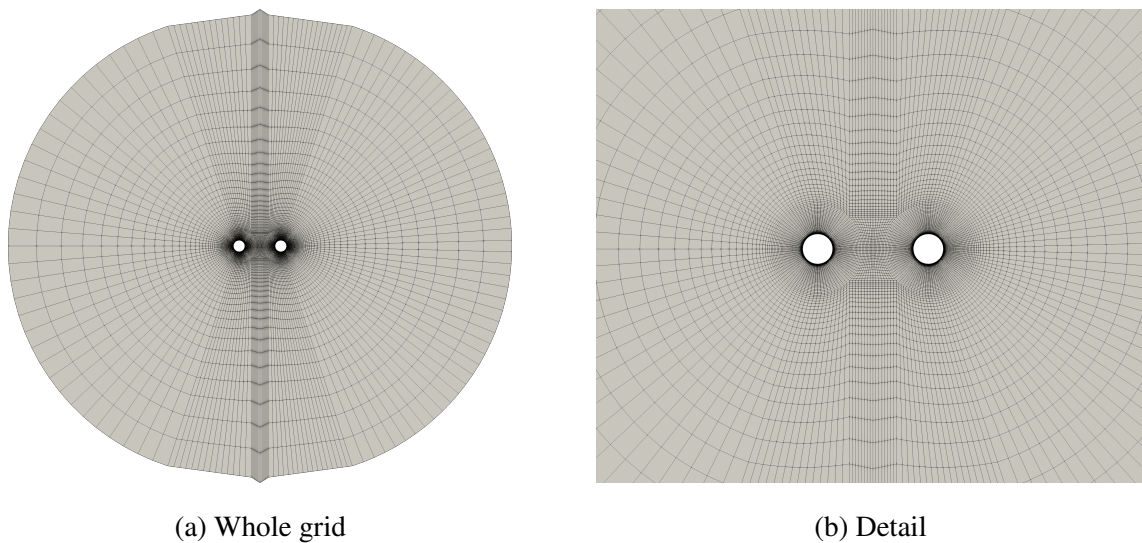


Fig. 1. Computational mesh used for the tandem cylinder problem

4. Problem description

As mentioned above, the solved test case is given by two identical cylinders in a row, with $D = 0.05715$ m being their diameter, while their centres are $3.7D$ away from each other. The free stream velocity is 44 m s^{-1} . As in [15], the prescribed inlet turbulence intensity is 4 %.

As the computational domain is symmetrical in the direction of the cylinder axes, the computational grid is composed of 30 layers (60 layers were also tested and no significant differences in results were found), each with the same structure and thickness of $0.025D$. One layer of this grid is depicted in Fig. 1, consisting of 17 725 cells. The chosen resolution is relatively rough, but the LES regions still comfortably satisfy the condition that more than 80 % of the turbulent kinetic energy is resolved, even though this is not a strict or necessarily always sufficient rule. The cells adjacent to the cylinders (no-slip walls, with zero velocity at their surface) also satisfy the condition for the dimensionless wall distance $y^+ < 1$. The inlet boundary is on the left side, the outlet is on the right side and the boundary condition chosen for the top and bottom of the domain is symmetry.

5. Results

The computed results of vortex shedding on the described tandem cylinders can be visualized by Mach number in the central horizontal cross-section, shown in Fig. 2, which also demonstrates some differences between the delayed hybrid models based on SST and TNT.

The hybrid methods also switched differently between RANS and LES modes. The values of the switches averaged over time are shown in Fig. 3. The basic DES and X-LES methods switched significantly more into LES mode in this test, while SST-DDES and SST-IDDES used LES mode slightly less. The DX-LES and especially IDX-LES switched into LES mode significantly less, but still retaining the regions with detached eddies in LES mode.

All the used methods can be compared with experimental data from [6, 7]. One of the quantities that can be compared are the pressure coefficients averaged over time shown in Fig. 4 for the front cylinder and Fig. 5 for the rear cylinder, which expands upon the results published in [5]. The results on the front cylinder show relatively good agreement with the experimental data, while the SST-based methods being slightly closer, with the notable exception of the

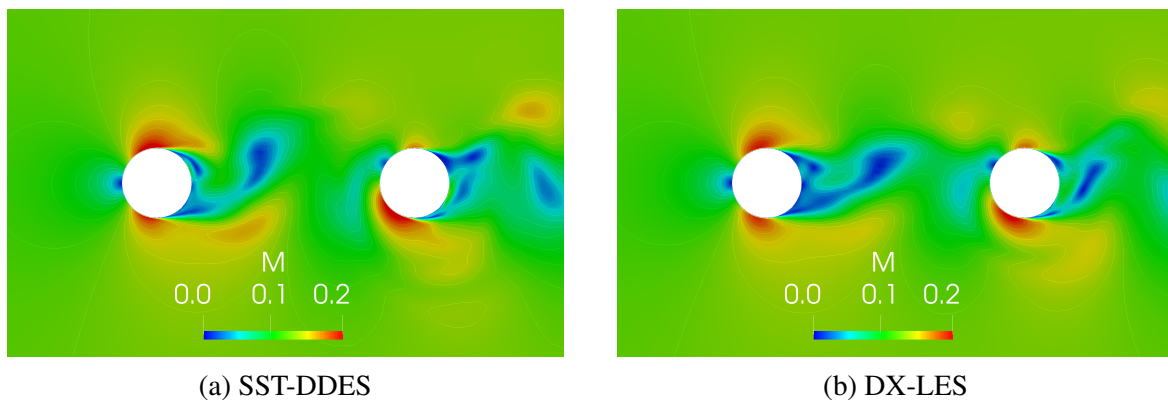


Fig. 2. Mach number calculated by different delayed hybrid models; similar phases are shown

IDDES model. The more important results, however, are on the rear cylinder. The data shows that the SST-IDDES model was significantly closer to the experimental measurements than the other SST-based methods, while the TNT-based models were closer overall, with DX-LES mostly closely matching the experimental data. It is also worth noting that some oscillations

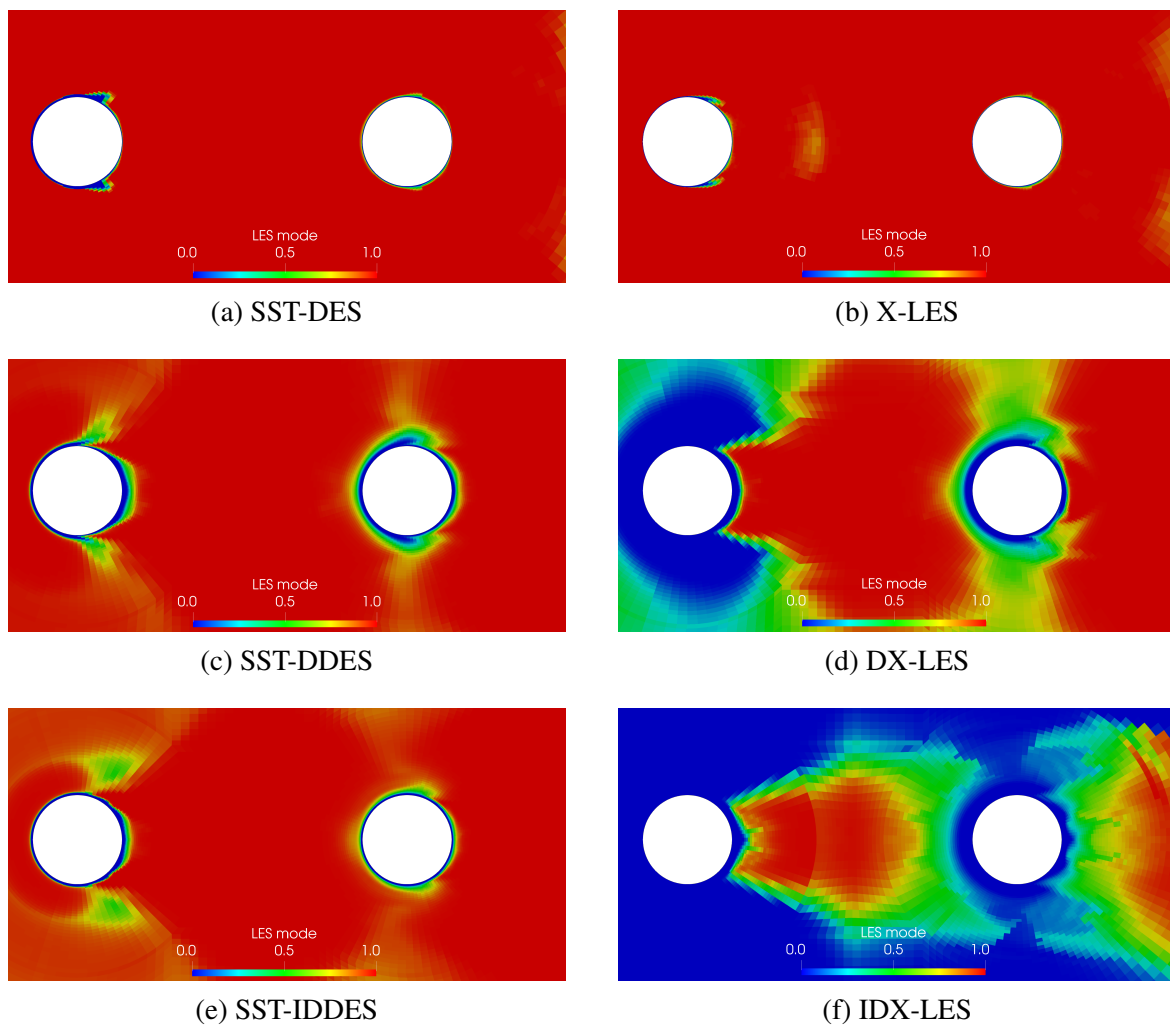
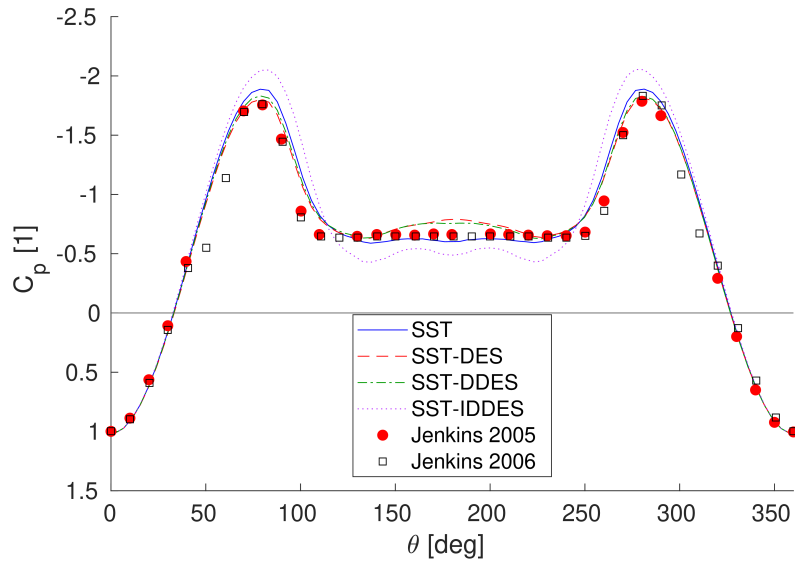
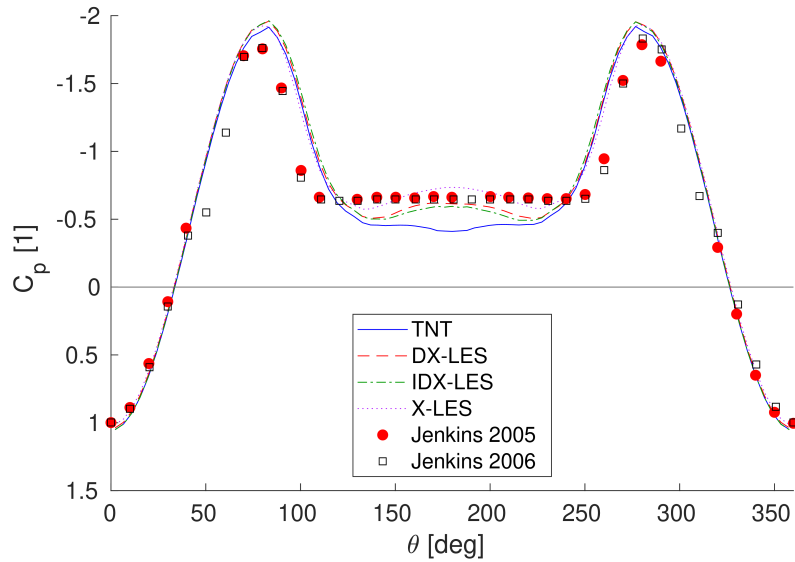


Fig. 3. Time-averaged RANS-LES switching of different hybrid methods – value of 0 indicates RANS-only mode, while 1 means full LES mode



(a) SST-based

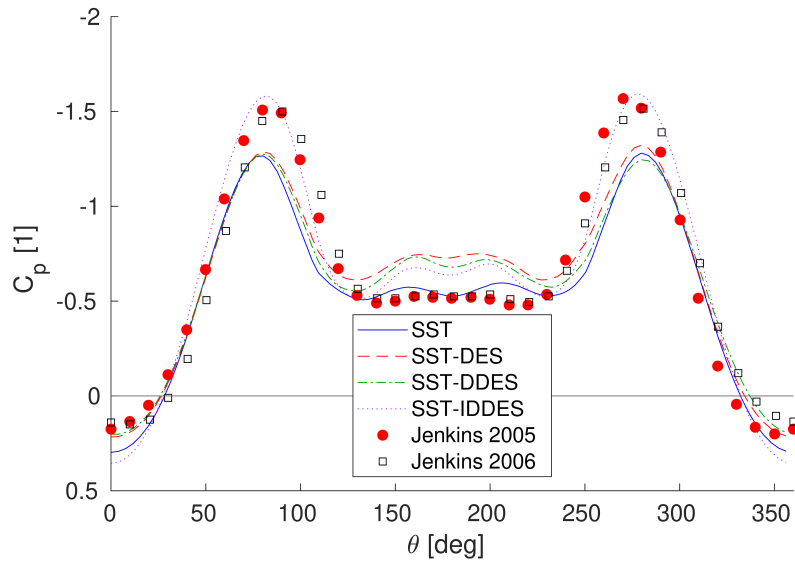


(b) TNT-based

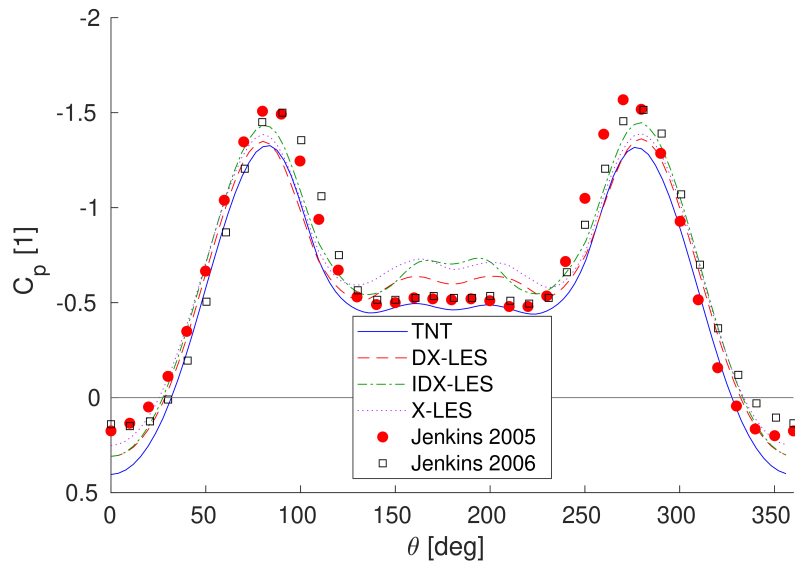
Fig. 4. Time-averaged calculated pressure coefficients on the *front* cylinder; the front of the cylinder is at $\theta = 0^\circ$, experimental data taken from [6, 7]

in the computed data are present in the area on the rear cylinder after the separation occurs, where the pressure coefficient is expected to be constant. These oscillations are more apparent in the results of the hybrid models, for which the flow is more dominated by fluctuations. This is especially the case on the rear cylinder, where the shedding frequency is different than on the front cylinder, and where the base RANS models are closer to the experimental data, as the oscillations in their evaluations are smaller. However, these deviations might be caused not only by the used methods, but also by the sampling frequency of the data used for averaging.

Another available experimental data are the averaged longitudinal fluid velocities in the middle of the domain (on the axis intersecting the centers of both cylinders), shown in Fig. 6. The computed data show a mismatch with the measurements from [7] in the area between the two cylinders, but correspond better to the measurements from [6] behind the second cylinder.



(a) SST-based



(b) TNT-based

Fig. 5. Time-averaged calculated pressure coefficients on the rear cylinder; the front of the cylinder is at $\theta = 0^\circ$, experimental data taken from [6, 7]

While from the SST-based methods only IDDES matches the experiment accurately in this region (except in the area right next to the cylinder), other of these methods correspond less to the experiment. The situation is different for the TNT-based models, for which only the X-LES model severely underpredicts the fluid velocity, while others show good agreement with the measurements, especially the DX-LES and IDX-LES models.

The last comparison with the experimental data are the computed values of the Strouhal number. The evaluation of the computed data for this value was done in a point exactly in the middle between the cylinders where the frequency of periodic pressure changes was studied. The results are shown in Table 2. Unfortunately, only one value of the Strouhal number was available from the experiments. The data show that the closest method to the measurements was the DX-LES model, followed by SST-IDDES.

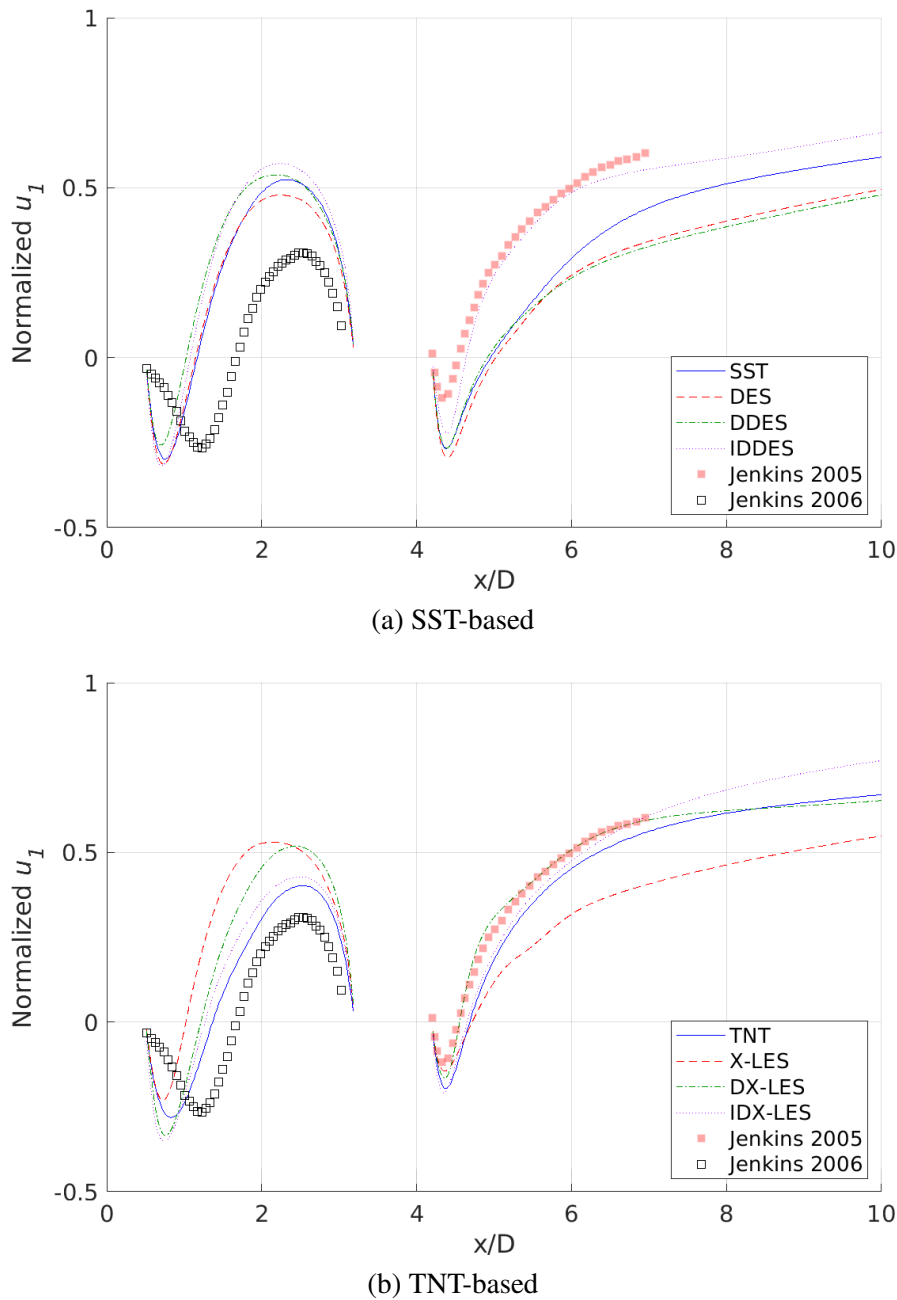


Fig. 6. Averaged longitudinal fluid velocities on the x -axis intersecting the centers of both cylinders for different x coordinates ($x = 0$ corresponds to the center of the first cylinder); coordinates are scaled proportionally to the cylinder diameter D and velocities in the direction of the x -axis to the free stream velocity 44 m s^{-1} ; the experimental data are from [6, 7]

Finally, vorticity contours for different models are shown. The results obtained by the TNT RANS method can be seen in Fig. 7. It is apparent by the symmetry in the direction parallel to the cylinder axes that the RANS method is, unlike the RANS-LES hybrid models, unable to capture the fluctuations properly. The results for the delayed variants (from the same time as in Fig. 2) are shown in Fig. 8. Although the hybrid methods show much less regular structures, it is worth noting that the computational meshes used are quite coarse, and the HLLC scheme is dissipative. As a result, the isosurfaces are not as rich as in the case of some of the cited sources (e.g., [15]).

Table 2. The values of the Strouhal number obtained by the turbulence models and by the experimental measurements from [6]

Method	Strouhal number
Experiment	0.24100
SST	0.22831
TNT	0.22816
SST-DES	0.21698
SST-DDES	0.22098
SST-IDDES	0.24742
X-LES	0.23028
DX-LES	0.23583
IDX-LES	0.22032

6. Conclusions

The described RANS and RANS-LES hybrid methods were compared on the tandem cylinder test case. The hybrid methods show improvement over the base RANS models in most of the data shown, especially the variants with non-binary switching.

The newly proposed DX-LES and IDX-LES show promise as their results for vortex shedding with reattachment and another detachment of the boundary layer are in good agreement with the experimental data, especially in the case of the DX-LES model, which is very close to the experimental data in most of the presented comparisons and outperforming other methods including its SST-counterpart. Moreover, in the DX-LES method, only the blending function is dependent on the distance from the nearest wall.

In the future, more tests should be done with these methods and the oscillations on the back of the cylinder should be further investigated. Also, another possible way of improving the newly introduced methods might be calibration of their model constants, although the models did not seem to need it in the tests carried out in this paper.

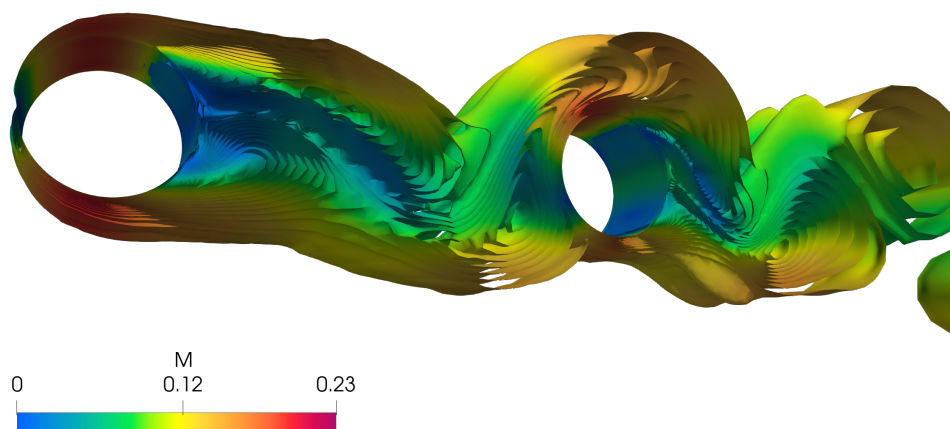
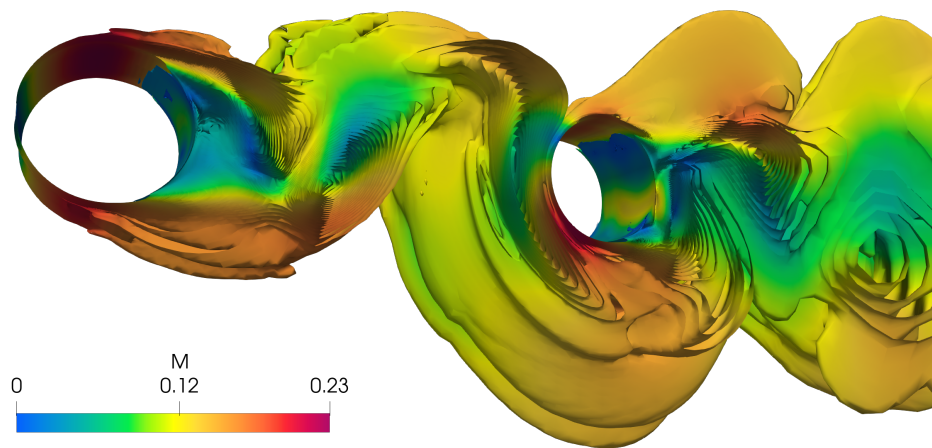
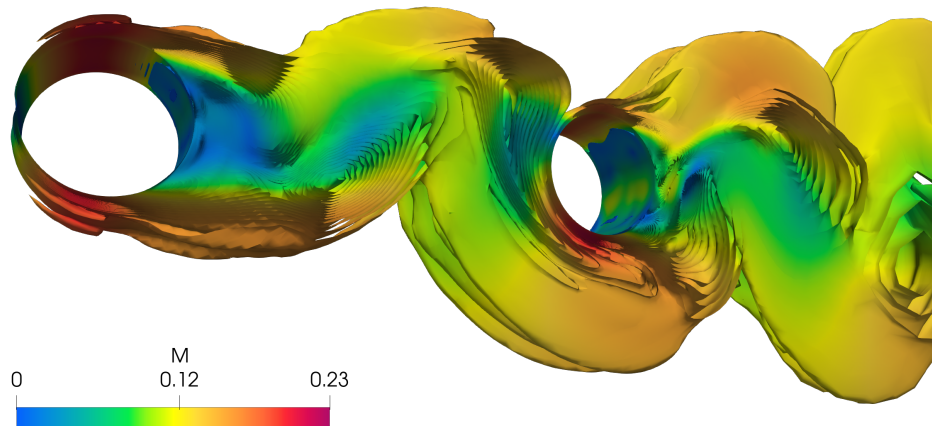


Fig. 7. Vorticity contours colored by computed velocities obtained by the TNT RANS model



(a) SST-DDES



(b) DX-LES

Fig. 8. Contours of vorticity colored by calculated Mach number obtained by the delayed DES models at similar phases

Acknowledgement

The financial support for this project was partly provided by the SGS22/148/OHK2/3T/12.

References

- [1] Fracassi, A., De Donno, R., Ghidoni, A., Noventa, G., Implementation and validation of the SST delayed eXtra-LES model for complex turbulent flows, *International Journal of Computational Fluid Dynamics* 36 (6) (2022) 441–464. <https://doi.org/10.1080/10618562.2022.2152013>
- [2] Frendi, A., Sun, Y., Noise radiated from two cylinders in tandem arrangement using high-order multidomain spectral difference method, *Proceedings of the 15th AIAA/CEAS Aeroacoustics Conference (30th AIAA Aeroacoustics Conference)*, 2009, pp. 1–18. <https://doi.org/10.2514/6.2009-3159>
- [3] Gritskevich, M. S., Garbaruk, A. V., Schütze, J., Menter, F. R., Development of DDES and IDDES formulations for the $k-\omega$ shear stress transport model, *Flow, Turbulence and Combustion* 88 (2012) 431–449. <https://doi.org/10.1007/s10494-011-9378-4>
- [4] Holman, J., Fürst, J., Rotated-hybrid Riemann solver for all-speed flows, *Journal of Computational and Applied Mathematics* 427 (2023) No. 115129. <https://doi.org/10.1016/j.cam.2023.115129>

- [5] Hájek, L., Karel, J., Klíma, M., Trdlička, D., Resolving flow around tandem cylinders with RANS-LES hybrid methods, Proceedings of the conference Computational Mechanics 2023, Srní, 2023, pp. 59–62.
- [6] Jenkins, L., Khorrami, M., Choudhari, M., McGinley, C., Characterization of unsteady flow structures around tandem cylinders for component interaction studies in airframe noise, Proceedings of the 11th AIAA/CEAS Aeroacoustics Conference, Monterey, 2005, pp. 1–18. <https://doi.org/10.2514/6.2005-2812>
- [7] Jenkins, L., Neuhart, D., McGinley, C., Khorrami, M., Choudhari, M., Measurements of unsteady wake interference between tandem cylinders, Proceedings of the 36th AIAA Fluid Dynamics Conference and Exhibit, San Francisco, 2006, pp. 1–18. <https://doi.org/10.2514/6.2006-3202>
- [8] Khorrami, M., Choudhari, M., Jenkins, L., McGinley, C., Unsteady flowfield around tandem cylinders as prototype for component interaction in airframe noise, Proceedings of the 11th AIAA/CEAS Aeroacoustics Conference, Monterey, 2005, pp. 1–22. <https://doi.org/10.2514/6.2005-2866>
- [9] Kok, J. C., Resolving the dependence on freestream values for k - ω turbulence model, Notes on Numerical Fluid Mechanics and Multidisciplinary Design, Springer 38 (7) (2000) 1 292–1 295. <https://doi.org/10.2514/2.1101>
- [10] Kok, J. C., Dol, H., Oskam, B., van der Ven, H., Extra-large-eddy simulation of massively separated flows, Proceedings of the 42nd AIAA Aerospace Sciences Meeting and Exhibit, Reno, 2004, pp. 1–12. <https://doi.org/10.2514/6.2004-264>
- [11] Köhler, F., Maduta, R., Krumbein, B., Jakirlić, S., Scrutinizing conventional and eddy-resolving unsteady RANS approaches in computing the flow and aeroacoustics past a tandem cylinder, In: New Results in Numerical and Experimental Fluid Mechanics XII, 2020, pp. 586–596. https://doi.org/10.1007/978-3-030-25253-3_56
- [12] Lockard, D. P., Summary of the tandem cylinder solutions from the benchmark problems for airframe noise computations–I workshop, Proceedings of the 49th AIAA Aerospace Sciences Meeting and Aerospace Exposition, Orlando, 2011, pp. 1–22. <https://doi.org/10.2514/6.2011-353>
- [13] Lockard, D. P., Choudhari, M. M., Khorrami, M. R., Neuhart, D. H., Hutcheson, F. V., Brooks, T. F., Stead, D. J., Aeroacoustic simulations of tandem cylinders with subcritical spacing, Proceedings of the 14th AIAA/CEAS Aeroacoustics Conference (29th AIAA Aeroacoustics Conference), Vancouver, 2008, pp. 1–16. <https://doi.org/10.2514/6.2008-2862>
- [14] Lockard, D. P., Khorrami, M. R., Choudhari, M. M., Hutcheson, F. V., Brooks, T. F., Stead, D. J., Tandem cylinder noise predictions, Proceedings of the 13th AIAA/CEAS Aeroacoustics Conference (28th AIAA Aeroacoustics Conference), Rome, 2007, pp. 1–26. <https://doi.org/10.2514/6.2007-3450>
- [15] Maduta, R., Ullrich, M., Jakirlic, S., Reynolds stress modelling of wake interference of two cylinders in tandem: Conventional vs. eddy-resolving closure, International Journal of Heat and Fluid Flow 67 (2017) 139–148. <https://doi.org/10.1016/j.ijheatfluidflow.2017.07.012>
- [16] Menter, F., Kuntz, M., Langtry, R. B., Ten years of industrial experience with the SST turbulence model, Heat and Mass Transfer 4 (2003) 625–632.
- [17] Nikitin, N. V., Nicoud, F., Wasistho, B., Squires, K. D., Spalart, P. R., An approach to wall modeling in large-eddy simulations, Physics of Fluids 12 (7) (2000) 1 629–1 632. <https://doi.org/10.1063/1.870414>
- [18] Schwaborn, D., Strelets, M., ATAAC – An EU-project dedicated to hybrid RANS-LES methods, Notes on Numerical Fluid Mechanics and Multidisciplinary Design 117 (2012) 59–75.
- [19] Spalart, P. R., Allmaras, S. R., A one-equation turbulence model for aerodynamic flows, Proceedings of the 30th Aerospace Sciences Meeting and Exhibit, Reno, 1992, pp. 1–22. <https://doi.org/10.2514/6.1992-439>

- [20] Spalart, P. R., Deck, S., Shur, M. L., Squires, K. D., Strelets, M., Travin, A., A new version of detached-eddy simulation, resistant to ambiguous grid densities, *Theoretical and Computational Fluid Dynamics* 20 (2006) 181–195. <https://doi.org/10.1007/s00162-006-0015-0>
- [21] Spalart, P. R., Jou, W. H., Strelets, M., Allmaras, S., Comments on the feasibility of LES for wings, and on a hybrid RANS/LES approach, *Proceedings of the 1st AFOSR international conference on DNS/LES*, 1997, pp. 137–148.
- [22] Strelets, M., Detached eddy simulation of massively separated flows, *Proceedings of the 39th Aerospace Sciences Meeting and Exhibit*, Reno, 2001, pp. 1–18.
<https://doi.org/10.2514/6.2001-879>
- [23] Wallin, S., Engineering turbulence modeling for CFD with a focus on explicit algebraic Reynolds stress models, Ph.D. thesis, Royal Institute of Technology, Stockholm, Sweden, 2000.
- [24] Weinmann, M., Sandberg, R. D., Doolan, C., Tandem cylinder flow and noise predictions using a hybrid RANS/LES approach, *International Journal of Heat and Fluid Flow* 50 (2014) 263–278.
<https://doi.org/10.1016/j.ijheatfluidflow.2014.08.011>